

# Theoretical and Experimental Studies on the Cut Zone Generated by AWJ Process

**I. Patirnac**

Lecturer Ph.D.  
Petroleum-Gas University of Ploiesti  
Faculty of Mechanical and Electrical  
Engineering  
Romania

**R. G. Ripeanu**

Professor Ph.D.  
Petroleum-Gas University of Ploiesti  
Faculty of Mechanical and Electrical  
Engineering  
Romania

**I. N. Ramadan**

Lecturer Ph.D.  
Petroleum-Gas University of Ploiesti  
Faculty of Mechanical and Electrical  
Engineering  
Romania

*The aim of this paper is to make a theoretical and experimental study to evaluate the water jet influence on a metallic material used in oilfield manufacturing, using AWJ process. It was investigated how the scattering of the jet has influenced the width of the kerf and neighboring area. The metallic material is P275NL2 which is a low temperature quality steel alloy specially used in petrochemical industry. The experimental tests were made on the waterjet cutting machine model YCWJ-380-1520 using pre-establish working conditions. Theoretical investigations were performed using CFD simulation with planar 2D fluid flow on the geometrical model. Graphical correlation was performed between theoretical outcomes given by CFD simulation and experimental results on the regarded material, overlapping on the theoretical searching for the cutting velocity and the hardening velocity limits nearby the kerf.*

**Keywords:** waterjet, kerf width, standoff, velocity, hardness, CFD.

## 1. INTRODUCTION

Due to its advantages over machining 2D geometrical shape with minimal waste of material, the AWJ process is widely used in oilfield equipment manufacturing and compared with plasma and laser cutting technology its accuracy has several advantages in manufacturing process [1, 2].

It is known that there are a lot of parameters which influence the AWJ process and any change of them can cause significant modification, both of the process itself and material quality. The surface quality of ductile material obtained using AWJ process is related by the kinetic energy of particles and interaction between these particles and mechanical properties of the material. Also, process parameters, like traverse speed, abrasive flow rate, standoff distance and water pressure have important effect on surface quality [3].

Research was performed using AWJ machine WUXI YCWJ-380-1520, with HPN orifice 0.25mm and 0.76mm on MT. Abrasive material used is Garnet 80Mesh and according to experimental measurements the shape factor 0.622 was obtained for abrasive particles. Water pressure developed by AWJ Machine is 280 MPa and abrasive flow rate was set to 4.5 g/s.

CFD simulation of the plain jet was performed regarding flowing parameters, like water velocity, obtained in previous flowing simulation on active parts of AWJ Machine. At the end of MT, it was obtained the average velocity of water to be about 187 m/s. According to some researchers [4, 5], the water velocity along to the mixing tube is between 120 and 400 m/s.

To study the plain jet, it was regarded that water velocity distribution is given by Gauss Bell shape [6-8].

The maximum water velocity is obtained along jet axis and the influenced area is larger as much as mixing tube leaves material surface.

According to these, the paper has the main purpose to perform correlation between CFD simulation and experiment to establish the velocity which produces the cutting and hardening of P275NL2 material steel used in petrochemical industry.

## 2. THEORETICAL INVESTIGATION OF KW USING CFD SIMULATION

Due to the turbulences flow, the spare jet shows divergent shape, and the extended diameter is proportional to standoff distance. According to some authors, the water velocity distribution for a plain jet it is performed with the respect of Gaussian bell, as formula (1) [6]: In this formula,  $v_{max}$  represents the maxim velocity value of water [m/s];  $r$ , means the extension radius of spare jet [m];  $x$ , the distance measured upward of waterjet upon a virtual source [m].

$$v(x, r) = v_{max} \cdot \exp\left(-\frac{50r^2}{x^2}\right) \quad (1)$$

The region between mixing tube orifice and piece surface has a large influence on material quality of AWJ process. For this purpose, a CFD simulation was performed using Fluent from Ansys Workbench to study water velocities variation and abrasive fluid behavior in that region. The main flowing parameter of the model is water velocity on mixing tube outlet, set to 200 m/s. That value was adopted from previous CFD simulation based on real experiment measurements. Consulting reference [9, 10], it a transient time and multiphase flow-2D was set, Euler, regarding two fluid phases, the primary phase was water set at the inlet of MT, and secondary is the air for the environment. In this study only a liquid phase presents interest in analyzing,

Received: June 2021, Accepted: September 2021

Correspondence to: Dr Iulian Patirnac  
Faculty of Mechanical and Electrical Engineering,  
Bld. Bucuresti 39, 100680 Ploiesti, Romania  
E-mail: ipatirnac@gmail.com

doi:10.5937/fme2104997P

© Faculty of Mechanical Engineering, Belgrade. All rights reserved

FME Transactions (2021) 49, 997-1004 997

considering that solid particles are united with the water stream.

The waterjet flowing was simulated in a spare region of 70 mm against a solid wall and the obtained water velocity contour is presented in Figure 1. The entire model was meshed using quadrat elements so that to simulate as possible as it can the real behavior of flowing, resulting in 1665 elements with 1799 nodes. As can be seen, the waterjet has a diverging structure since water particles tend to minimal resistance regions like atmospheric pressure of environment. The maximum velocity value is about 214 m/s and it is constant along jet axis up to the wall where stagnation zone is acting.

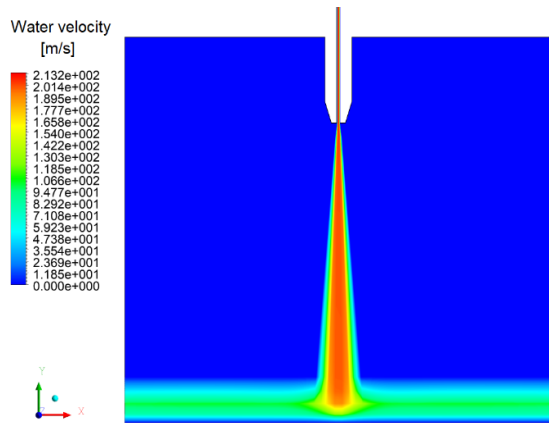


Figure 1. Contour of water in CFD simulation [11]

The graphical shape of water velocity up to 4 mm standoff distance resulted within a pale of CFD simulation as presented in Figure 2.

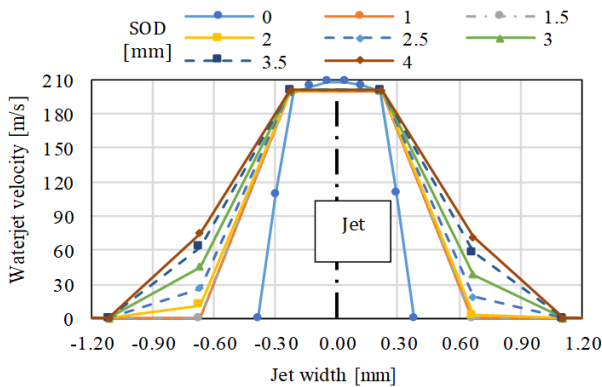


Figure 2. Water velocity distribution according to CFD simulation [11]

It can be noticed that all graphics present a Gauss Bell feature, except for MT outlet where distribution of water velocity is characterized by turbulent flow. Also, for all distributions it was recorded that maximum value of velocity to about 200 m/s is on an aperture of 0.21 mm from jet axis. The jet influence can be distinguished where water velocity increases, which means that in case of 1mm above the material surface water velocity can be regarded up to 0.667 mm from jet axis and in case of 4mm standoff it is about 1.1 mm.

### 3. EXPERIMENTAL INVESTIGATION OF KW

For experimental investigation of kerfs the schematic of sample presented in Figure 3 was adopted. To highlight

the AWJ influence on kerfs, four stages of MTH, five values of SOD and transversal speed rate of about 4mm/min were regarded.

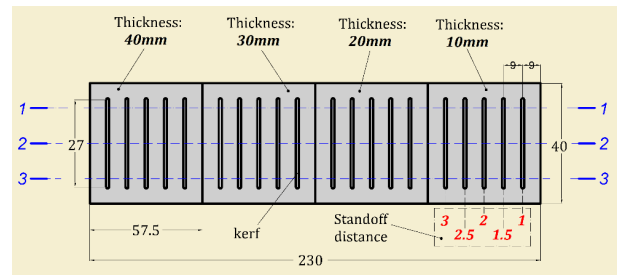


Figure 3. Schematic of material sample [11]

Due to some factors of material uniformity, like remanent stresses, the AWJ process was performed along 27mm and 9mm between kerfs, without material exit along traverse moving on the axis.

The material used for experiment is P275NL2, a soft alloyed steel used for high pressure equipment, containing 0.17% C and the yield strength is about 275MPa, according to standard [12].

### 3.1 Kerf width analysis

For geometrical investigation of KW were performed measurements using optical instruments included, both at the entrance of the jet to the material and to the exit, since kerf geometry presents the tapering shape [13]. Measured values of KW in the upper region are presented in Table 1. Due to material thickness, it has a low influence on kerf width generation in the upper zone. The average of measured values obtained for each SOD were calculated.

Table 1. KW values on top region,  $w_s$  [mm] [11]

MTH [mm]	Standoff distance [mm]				
	1.0	1.5	2.0	2.5	3.0
10	0.895	0.923	0.980	1.007	1.089
20	0.867	0.894	0.868	0.927	1.047
30	0.845	0.901	0.957	0.998	1.039
40	0.829	0.899	0.928	0.946	1.034
Average	0.859	0.904	0.933	0.969	1.052

Figure 4 depicts the graphical representation of width kerf variation at the entrance of the jet through the material, according to SOD.

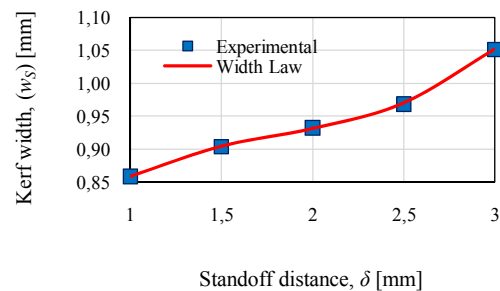


Figure 4. KW variation on top region [11]

As can be noticed, KW in the top region presents an increasing variation tendency as much as the MT leaves the material surface. This fact occurs due to the jet of

water diverge with the increase of SOD and the influenced material area by particles impingement becomes larger in its turn. The measured values of KW at the bottom of material are presented in Table 2.

**Table 2. KW values on lower region,  $w_i$  [mm] [11]**

MTH [mm]	Standoff distance [mm]					Average
	1.0	1.5	2.0	2.5	3.0	
10	0.926	0.919	0.927	0.943	0.967	0.936
20	0.942	0.956	0.978	1.005	1.023	0.981
30	1.006	1.023	0.979	0.971	0.976	0.991
40	0.922	0.897	0.924	0.782	0.892	0.883

In KW study at the bottom of the material the average of standoffishness was performed, since the distance between the surface material and MT orifice has minor influence on cutting width to the bottom of the material.

The graphical representation of KW variation with respect of material thickness to the bottom of the sample is depicted in Figure 5. As can be noticed, the kerf width increases up to 30mm depth and after decreases with a high slope up to 40mm depth. According to some authors [14], this fact occurs since there are two mechanisms of wear which rule the AWJ process along jet trajectory inside the material. So, the upper zone is characterized by cutting wear and the lower zone by deformation wear. The kerf is tighter but more distorted to the bottom of the material since jet deflection is more visible in this region.

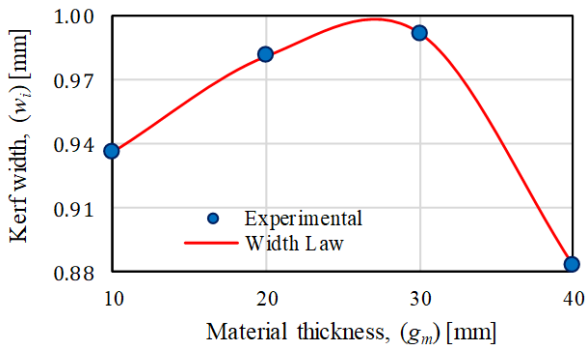


**Figure 5. KW variation on bottom region [11]**

Concerning graphical distribution, the equations which govern the kerf formation process were developed. It was obtained that kerf width to upper region is varying with polynomial distribution given by relation (2) and to the bottom, according to relation (3) [11]. In both cases a fitting around 99% was obtained between tendency curves and experimental.

$$w_s = 0.042 \cdot \delta^3 - 0.228 \cdot \delta^2 + 0.463 \cdot \delta + 0.5814 \quad (2)$$

$$w_i = 1.002 - 4.78 \cdot 10^{-19} \cdot \exp(g_m) - 2.869 \frac{\ln(g_m)}{g_m^2} \quad (3)$$

In the above formula,  $w_s$  and  $w_i$  mean the kerf width at top of material respectively to the bottom [mm],  $\delta$  represents the distance from surface material to mixing tube orifice [mm] and  $g_m$  is material thickness [mm].

For a clearer KW variation to the outlet area of the jet from the material, it was proceeded to its spatial representation depending on the SOD and the depth of

penetration of the jet into the material, as shown in Figure 6.

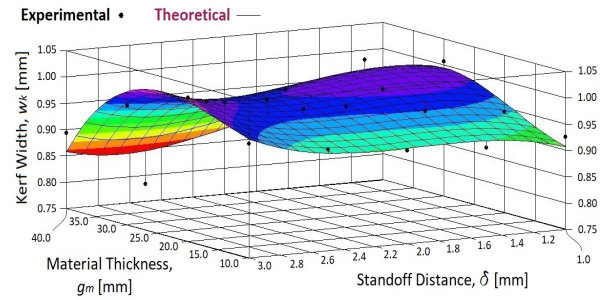


**Figure 6. Spatial representation of KW [11]**

It can be noticed that the dependence of the KW with respect to MTH is like the curve presented in Figure 5. As regarding the KW with respect to SOD, graphical representation on spatial coordinates is not so suitable in the range of MTH between 20-40 mm. Analytical dependence of KW in spatial coordinates for P275NL2 steel is given by equation (4) and coefficient of determination  $R^2=0.794$ .

$$w_0 = 0.69 - 8.57 \cdot 10^{-3} \cdot g_m + 0.452 \cdot \delta + 8.33 \cdot 10^{-4} \cdot g_m^2 - 0.242 \cdot \delta^2 + 8.165 \cdot 10^{-4} \cdot g_m \delta - 1.4 \cdot 10^{-4} \cdot g_m^3 + 0.041 \cdot \delta^3 + 2.62 \cdot 10^{-4} \cdot \delta^2 g_m - 8.4 \cdot 10^{-5} \cdot \delta g_m^2 \quad (4)$$

The analytical relations obtained in KW study can be used to optimize process parameters, like SOD and material thickness, to obtain the required quality of regarded material, using AWJ process.

### 3.2 Kerf tapering analysis

Considering the results obtained by various researchers [15, 16], as well as the results from this study, it was noticed that the shape of the cut obtained by AWJ process is not perfectly straight, it can be either convergent ( $w_s > w_i$ ) or divergent ( $w_s < w_i$ ), as shown in Figure 7.

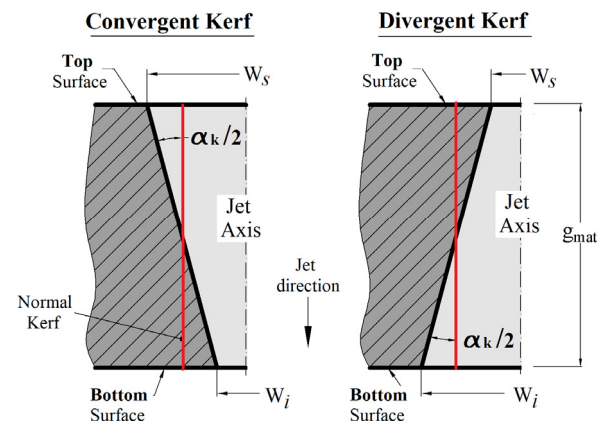


**Figure 7. Kerf Tapering [11]**

Knowing the values of KW previously depicted, it was established KT and KTA using formulas given by the relation (5) and (6). Due to KT and KTA analytically related, graphical representation of both, depending on SOD have the same shape, excepting only the values of angles.

$$C = \frac{w_s - w_i}{g_{mat}} \quad (5)$$

$$\alpha_k = \frac{360}{\pi} \tan^{-1} \left( \frac{C}{2} \right) \quad (6)$$

In the above formula,  $C$  is the kerf taper [ $\mu\text{m}/\text{mm}$ ], and  $\alpha_k$  represents the kerf-taper angle [deg].

The obtained values of the and KT and KTA performed on the P275NL2 steel are presented in Table 3, It can be noticed that in the case of positive sign of tapering the shape of the cut is convergent along jet axis, and divergent in the case of negative one.

**Table 3. KT and KTA values,  $C$  [ $\mu\text{m}/\text{mm}$ ] /  $\alpha_k$  [deg] [11]**

MTH [mm]	SOD, [mm]				
	1.0	1.5	2.0	2.5	3.0
10	-3.067	0.400	5.300	6.467	12.133
	-0.176	0.023	0.304	0.371	0.695
20	-3.767	-3.083	-5.483	-3.917	1.200
	-0.216	-0.177	-0.314	-0.224	0.069
30	-5.367	-4.056	-0.733	0.878	2.089
	-0.307	-0.232	-0.042	0.050	0.120
40	-2.333	0.067	0.083	4.100	3.550
	-0.134	0.004	0.005	0.235	0.203

In the case of AWJ machining at SOD of 1mm, the taper of the cuts is negative, which means a divergent shape, and at the maximum distance between the nozzle and the piece the taper value has the positive sign for all four MTH considered. Inside SOD interval, all graphical representations of tapering present an increasing distribution, except for 20mm MTH which is varying irregularly, as can be seen in Figure 8. That fact occurs due to material is not uniform along jet direction.

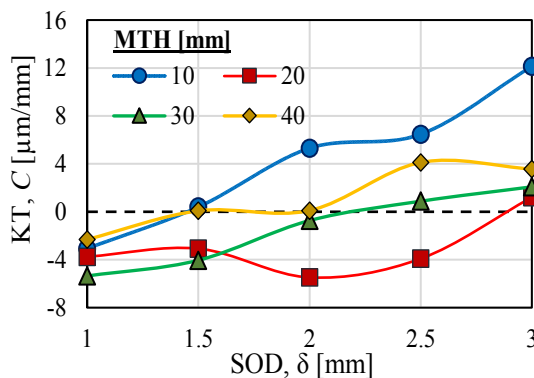


**Figure 8. Kerf Tapering Distribution [11]**

The maximum positive value is 12.1  $\mu\text{m}/\text{mm}$  processing the thickness of 10mm at SOD of 3mm, and the maximum negative value is 5.48  $\mu\text{m}/\text{mm}$ . The optimal values (those close to zero) were obtained for the MTH of 40mm at the SOD between 1.5-2mm. The furthest values from the normal were obtained in the case of 10mm MTH. In such case it is not recommended to use a soft feed-rate (4mm/min) in the case of thin parts machined by AWJ process.

### 3.3 Hardness investigation

There is an area near the cuts for which the impact velocity of the sand particles has no longer energy to

remove the material, but they have effect on the microstructural properties of the material. For this purpose, the area next to each cut was analyzed to observe the changes produced by the abrasive jet in terms of surface hardness.

For each sample, the Vickers hardness layer in the vicinity of the cut was measured, starting at 0.05 mm from the edge of the cut toward exterior (unaffected region) until the measured value reached or fell below the specific hardness of the material. The measurement interval between Vickers indenter marks was set to 0.07mm. Since Brinell hardness of P275NL2 steel was measured to be 167HB, by equivalence according [17], a Vickers hardness of 176HV resulted.

The Vickers test was performed according to the normative presented in [18], using microhardness tester Emcotest DuraScan 20, presented in Figure 9. For each sample was applied a load of 0.2 kgf.

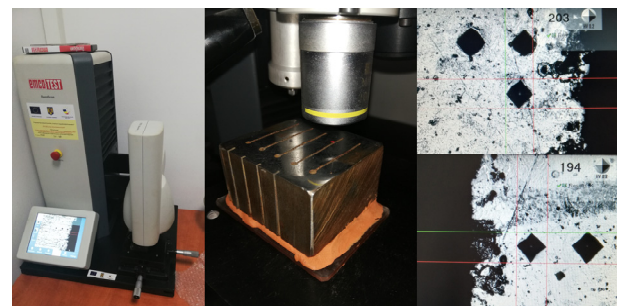


**Figure 9. Vickers Microhardness Test**

Values of Vickers hardness obtained in the vicinity of the cuts for 20 mm step thickness with respect to SOD, are presented in Table 4. For all samples, the measured values of hardness are around 190 – 200 HV for those in the vicinity of the cuts. Toward unaffected region, hardness values are between 160 – 170 HV, except for some values that come out of this range. It can be noticed that the upper layer of material is affected by particle impingement.

**Table 4. HV values for 20mm MTH [11]**

SOD, [mm]	Influenced length, [mm]					
	0.05	0.12	0.19	0.26	0.33	0.40
1.0	194	189	179	175	175	171
1.5	194	187	183	175	167	167
2.0	197	192	192	177	171	167
2.5	214	199	189	179	167	167
3.0	196	192	189	183	179	175

The hardness variation diagram in the influenced area in the case of the 20 mm MTH is presented in Figure 10.

The hardness values at 0.05 mm from the cutting edge are around 195 HV, except for 210 HV at distance of 2.5 mm from the part. The influence of the jet particles is active up to 0.242mm from the cutting edge in the case of 1mm SOD, and for 3 mm above from material surface the jet has an influence on the distance of 0.381 mm from the cutting edge. All influenced length values were obtained performing graphical representation, according to measurements of HV.

Values of influenced areas by the water jet, depending on the distance between the nozzle and the

surface of material, are presented in Table 5. Since the water jet has generally the same influence on the material surface, the arithmetic mean of distances from the cutting edge was calculated for the three MTH analyzed. The average value of the hardened layer in the case of 1mm SOD is 0.153mm away from the cutting edge, and in the case of 3mm above the material surface the value of 0.305mm was obtained.

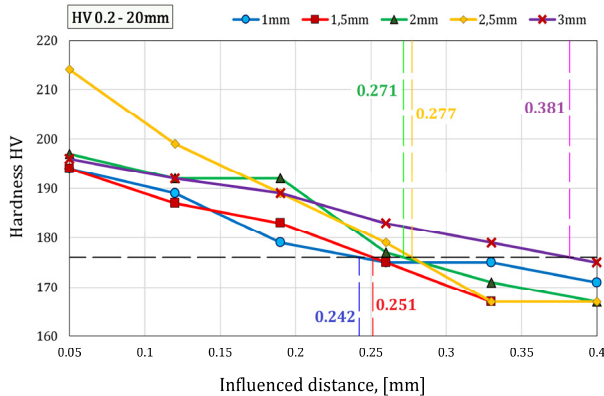


Figure 10. Hardness variation for 20mm MTH [11]

Table 5. Hardened layer width,  $w_h$  [mm] [11]

SOD, [mm]	MTH, [mm]			Average, $w_h$ [mm]	Including KW, [mm]
	20	30	40		
1.0	0.242	0.110	0.106	0.153	0.582
1.5	0.251	0.184	0.137	0.191	0.643
2.0	0.271	0.259	0.143	0.224	0.691
2.5	0.277	0.329	0.175	0.260	0.745
3.0	0.381	0.345	0.190	0.305	0.831

According to the values obtained in hardened layer of P275NL2 steel, the graphical variation of hardened width layer according to SOD was performed, as is presented in Figure 11.

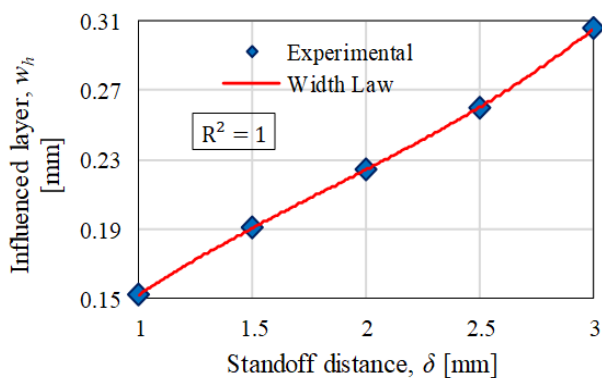


Figure 11. Chart of hardened layer width [11]

It can be noticed that the dependence of influenced area varies according to a third order polynomial function, whose equation is given by the relation (7) [11]. This law is valid only in the adjacent area of the cuts and does not take the KW into account.

$$w_h = 0.0092 \cdot \delta^3 - 0.0504 \cdot \delta^2 + 0.1591 \cdot \delta + 0.0347 \quad (7)$$

In the above formula,  $w_h$  is the hardened width layer [mm],  $\delta$  represents SOD, [mm].

#### 4. CORRELATIONS BETWEEN EXPERIMENTAL AND CFD SIMULATION

Using graphical distribution of water velocity obtained in CFD simulation, along with physical measurement of KW and Vickers hardness, were established particles velocities generated by AWJ process which produce cutting and hardening of steel P275NL2.

To establish the particle velocity which produce the material cutting of P275NL2, it was regarded the water velocities distribution generated by CFD simulation along with average values of cuts width obtained by real measurement, namely 0.859 mm and 1.052 mm for the extreme values of SOD of 1 mm, respectively 3 mm. By overlapping the cuts width on water velocities distribution, it was obtained the particles velocities which produce material cutting, presented in Figure 12. According to the investigation, the velocity of 104.66 m/s at distance of 1 mm from the part surface, and 95.66 m/s to 3 mm above was obtained. Normally, the cutting velocities should be equal irrespective of standoff distance and difference between them corresponds to an error of 9%. For the other values of standoff distance, it can be regarded those cutting velocities are placed inside hatched area.

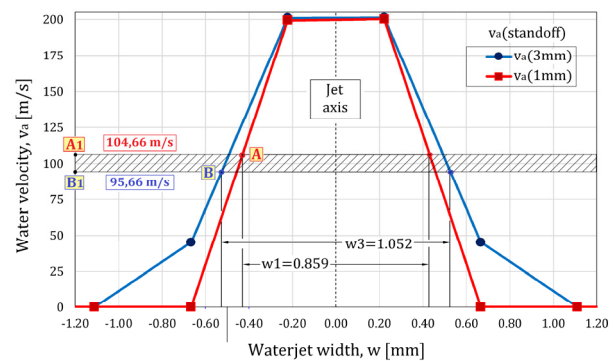


Figure 12. Cutting velocity diagram [11]

To establish the particles velocities which produce material hardening, it was regarded the graphical distribution of water velocities given by CFD simulation in case of 1 mm and 3 mm SOD, and average values of influenced material region, namely 0.153 mm and 0.305 mm. By overlapping the velocities distribution and hardness modification area, it was obtained the particles velocities which produce P275NL2 hardening, presented in Figure 13.

For the regarded material, it was obtained the particle velocity which produce hardening to be 36.685 m/s for 1 mm SOD and 27.956 m/s to 3 mm. As the first case, these hardening velocities values should be equal, but the difference between them would influence a region of 0.02 mm.

A metallography investigation of steel P275NL2 was performed near the cuts to establish the grain modification occurred during sand particles impingement of AWJ process. According to [19] was established the average grain size index (G) using comparison image with standard charts. It was investigated the metallographic structure by reelevating images for those affected regions nearby the cuts, presented in Figure 14, and unaffected region, presented

in Figure 15. According to SEM investigation magnification 250x was set for, and comparison factor of magnification 100x was adopted for each sample.

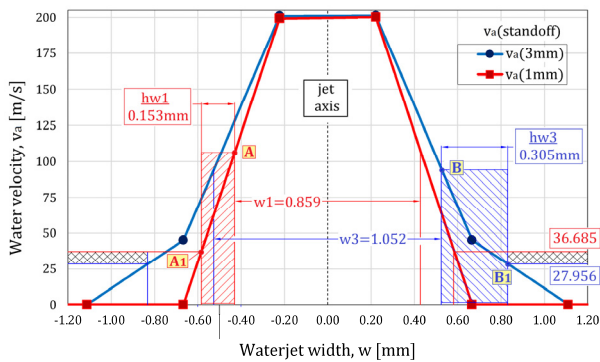


Figure 13. Hardening velocity diagram [11]

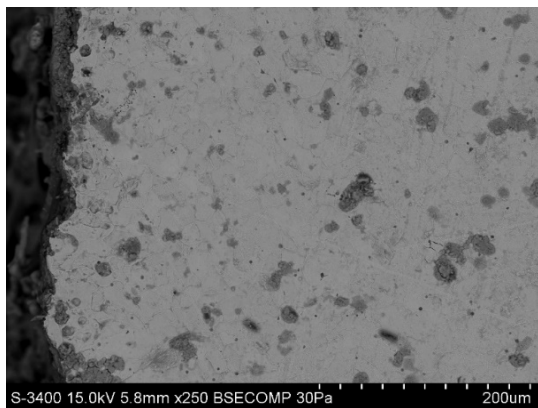


Figure 14. Metallographic image for affected region [11]

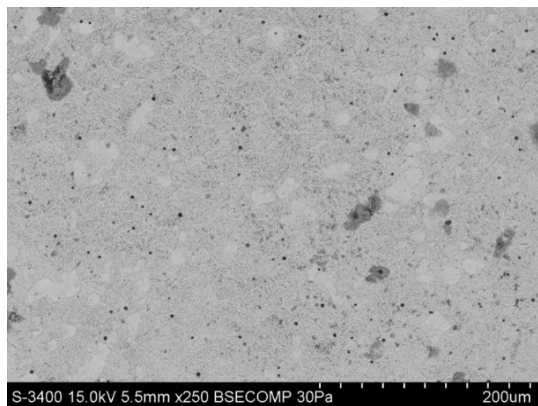


Figure 15. Metallographic image for unaffected region [11]

Since investigated image magnification is different from 100x, the mean grain size index was established using formula (8) [19]. In this formula,  $G_g$  represents the comparison grain size factor corresponding to magnification 100x, while  $g_n$  is magnification image screen used for metallographic samples (250x).

$$G = G_g + 6.64 \cdot \log\left(\frac{g_n}{100}\right) \quad (8)$$

Grain characteristics of P275NL2 obtained from microscopic analysis of the two regarded regions are presented in Table 6. The average diameter of grains was adopted using [20] and comparison index according to standard charts presented in [19].

Correlations between metallographic investigation of the grain size and Vickers hardness results specific to two areas of influence, are presented in Table 7. The percentage ratio between the affected and unaffected area of the two sizes is made.

Table 6. Grain characteristics modification [11]

	Affected region	Unaffected region
Comparison grain index, $G_g$ [-]	6	5.5
Grain size index, $G$ [-]	8.6	8.1
Average grain area, [ $\text{mm}^2$ ]	0.012	0.017
Number of grains, [grains/ $\text{mm}^2$ ]	3200	2263
Average grain diameter, [ $\mu\text{m}$ ]	18.9	22.5

Table 7. Characteristics modification of P275NL2 [11]

	Average hardness, HV	Grain size index, $G$ [-]
Affected region	192.13	8.6
Unaffected region	176	8.1
Percentage modification	8.39	5.78

The same study was performed in [21] for carbon steel subjected to Vanadium-Carbide coating process, using microhardness and SEM investigation of the layers. In this paper was noticed that substrate microhardness is significantly reduced (up to 30%) directly below the coating with respect of hardness of deeper substrate, while carburized region is modified up to 10%.

## 5. DISCUSSIONS

Both KT and KTA are influenced by MTH and the technological parameters of the process. An important factor is the nature of the processed material, as well as its degree of homogeneity. During AWJ process, it is important that cut section is as close as possible to the ideal conditions (tapering must be as small as possible). For P275NL2 steel it is recommended to adopt a high value of the feed-rate when processing small thicknesses of material, and the distance between the MT and the surface of the processed material to be between 1.5-2mm. Similar conclusions were obtained in the paper [22], where KW is reduced as feed-rate increases, whereas KTA has constant behaviour.

In the case of experimental tests presented in the paper [23], the same increasing dependence of the KW was obtained for MTH included in the range of 10-30mm. In this paper an acrylic material is processed using 1.33mm MT with SOD of 1mm and feed rate in range of 1-5 mm/s.

In reference [6] a layered com-po-site material consisting of carbon fibre (CFRP) and tita-nium alloy (Ti6Al4V) was processed. 0.76 mm MT, 0.25mm HPN, water pressure of 280 MPa was used, and the feed rate varying from 5 to 95 mm/min. When the titanium alloy is above CFRP, the cut configuration is "X" sha-ped, and when CFRP is above a barrel-shaped confi-guration was obtained. Compared with P275NL2, it can be concluded that in the case of divergent concities (negative KTA), the material had breaking CFRP behaviour, and in the case of positive KTA the material had

the behaviour of metallic materials with much more difficulty of machinability.

In terms of microstructure analysis, referring to work [24] it was AWJ processed Brass-353 using 1.27mm TM, 4mm SOD and feed-rate in range of 20-140 mm/min. It was stating that the water jet causes changes in the microstructure of the material, but without any effect on the hardness in the vicinity of the cut. This fact occurs due to Brass is machined using a feed-rate value much higher compared to steel presented in this paper. The feed-rate speed being high the impact of abrasive particle on material surface could be insignificant.

## 6. CONCLUSION

From CFD simulation it was obtained that maximum velocity value of water is around 200 m/s in the jet core and has influence on 0.21 mm per radius for all standoff distances. Up to 4mm above the piece, waterjet diverges up to 1.1 mm/radius and all velocities graphics present a Gauss bell shape like.

It was obtained that kerf wide at the top of P275NL2 steel is varying according to a polynomial distribution with standoff distance. To the bottom, the kerf width is influenced, especially by material thickness and varies according to an exponential distribution.

According to tapering investigation of kerfs, it was concluded that optimal SOD is around 1.5-2mm for high MTH (40mm), and in case of small MTH (10mm) it is not recommended to use slow feed-rate (4mm/min), kerf shape is much more divergent in this case.

It was obtained that the particles velocities which produce material cutting are in the range of 95.66 – 104.66 m/s, corresponding to 1-3mm standoff distance. It can be appreciated that for the other values of standoff, particles velocities can be placed inside the interval, according to CFD simulation.

From hardness investigation next to the kerf, it was obtained that the range of particles velocities which produce the material hardening are between 27.95 - 36.68 m/s, corresponding to 1 mm up to 3 mm above from piece surface. From metallic structure investigation it was obtained that grain size is modified with 5.78% next to the kerf and the influenced area is less than 0.305 mm from the cut edge. The influenced area is insignificant compared to other cutting processes where metallic structure is clearly modified.

Since CFD simulation was performed without regarding abrasive particle parameters, in subsequent study the influence of roundness and sharpness of abrasive particles on cutting process of P275NL2 using AWJ technology will be analyzed.

## REFERENCES

- [1] Akkurt, A., The effect of cutting process on surface microstructure and hardness of pure and Al 6061 aluminum alloy, *Engineering Science and Technology - International Journal*, Vol. 18, No.3, pp.303-308, 2015.
- [2] Mishra D.R., Gautam G.D., Prakash D., Bajaj A., Sharma A., Bisht R., Gupta S., Optimization of Kerf Deviations in Pulsed Nd:YAG Laser Cutting of Hybrid Composite Laminate Using GRA, *FME Transactions*, Vol. 48, No. 1, pp 109-116, 2020.
- [3] Marichamy S., Ravichandran M., Stalin B., Sridhar Babu B., Optimization of Abrasive Water Jet Machining Parameters for  $\alpha$ - $\beta$  brass using Taguchi Methodology, *FME Transactions*, Vol. 47, No. 1, pp 116-121, 2019.
- [4] Kamarudin, N.H., Prasada, R.A.K., Azhari, A., CFD Based Erosion Modelling of Abrasive Waterjet Nozzle using Discrete Phase Method, *IOP Conf. Series: Materials Science and Engineering*, 12-14.11.2015, Kuala Lumpur, Malaysia, vol.114.
- [5] Long X., Ruan X., Liu Q., Chen Z., Xue S., Wu Z., Numerical investigation on the internal flow and the particle movement in the abrasive waterjet nozzle, *Powder Technology*, vol. 314, pp. 635-640, 2017.
- [6] Alberti A., Artaza T., Suarez A., Rivero A., Girot F., An experimental study on abrasive waterjet cutting of CFRP/Ti6Al4V stacks for drilling operations, *International Journal of Advanced Manufacturing and Technology*, Vol. 86, pp.691–704, 2016.
- [7] Pahuja R., Ramulu M., Abrasive water jet machining of Titanium (Ti6Al4V)–CFRP stacks – A semianalytical modeling approach in the prediction of kerf geometry, *Journal of Manufacturing Processes*, Vol. 39, pp.327–337, 2019.
- [8] Li M., Huang M., Chen Y., Gong P., Yang X., Effects of processing parameters on kerf characteristics and surface integrity following abrasive waterjet slotting of Ti6Al4V/CFRP stacks, *Journal of Manufacturing Processes*, Vol. 42, pp.82–95, 2019.
- [9] Simulating a Jet Impingement in ANSYS Fluent using Eulerian Multiphase model, available at: <https://www.youtube.com/watch?v=VdEOglbypDY&t=523s>, accessed: 15.07.2019.
- [10] Zivkovic S., Milinovic M., Adamec N., Experimental and Numerical Research of a Supersonic Planar Thrust Vectoring Nozzle via Mechanical Tabs, *FME Transactions*, Vol. 42, No. 3, pp 205-211, 2014.
- [11] Patirnac I.: Researchers on Waterjet Manufacturing of the Metallic Materials Used in Petroleum and Petrochemical Industry, PhD Thesis, Mechanical PhD Domain, Petroleum-Gas University of Ploiesti, Ploiesti, 2020 (in Romanian).
- [12] EN 10028-3: 2009 Flat products made of steels for pressure purposes. Weldable fine grain steels, normalized.
- [13] Kishore S.J., Charan Teja P., Eshwariaha B., Harshvardhan Reddy K.: Experimental Control of Kerf Width Taper During Abrasive Water Jet Machining, *FME Transactions*, Vol. 47, No. 3, pp 585-590, 2019.
- [14] Cosansu G., Cogun C.: An investigation on use of colemanite powder as abrasive in abrasive waterjet

cutting (AWJC), Journal of Mechanical Science and Technology, Vol. 26, No. 8 pp. 2371 – 2380, 2012.

- [15] Gnanavelbabu A., Saravanan P., Rajkumar K., Karthikeyan S., Experimental Investigations on Multiple Responses in Abrasive Waterjet Machining of Ti-6Al-4V Alloy, ICMMM – 2017, Materials Today: Proceedings, vol. 5, pp. 13413–13421, 2018.
- [16] Shanmugam D.K., Wang J., Liu H., Minimisation of kerf tapers in abrasive waterjet machining of alumina ceramics using a compensation technique, International Journal of Machine Tools & Manufacture, vol. 48, pp. 1527–1534, 2008.
- [17] [https://www.engineeringtoolbox.com/bhn-brinell-hardness-number-d\\_1365.html](https://www.engineeringtoolbox.com/bhn-brinell-hardness-number-d_1365.html) (accessed: 21.02.2020).
- [18] SR EN ISO 6507-1:2018, Metallic materials - Vickers hardness test - Part 1: Test method, 2018.
- [19] EN ISO 643, Steels - Micrographic determination of the apparent grain size, 2020.
- [20] ASTM E112-10 Standard Test Methods for Determining Average Grain Size, 2010.
- [21] Hoffer G., Simunovic K., Samardzic I., Vidakovic I., Effect of Speed and Impact Angle on Solid Particle Erosion of Vanadium Carbide Coatings Produced by Thermo-Reactive Diffusion Technique, FME Transactions, Vol. 48, No. 3, pp 497-503, 2020.
- [22] Gudimetla P., Wang J., Wong W., Kerf formation analysis in the abrasive waterjet cutting of industrial ceramics, Journal of Materials Processing Technology, vol. 128, pp. 123–129, 2002.
- [23] Ma C., Deam R.T., A correlation for predicting the kerf profile from abrasive water jet cutting, Experimental and Thermal Fluid Science, Vol. 30, pp.337–343, 2006.
- [24] Akkurt A., Cut Front Geometry Characterization in Cutting Applications of Brass with Abrasive Water

Jet, Journal of Materials Engineering and Performance, vol. 19, no. 4, pp. 599-606, 2010.

## NOMENCLATURE

AWJ	Abrasive Waterjet
HPN	High Pressure Nozzle
MT	Mixing Tube (Focusing Tube)
CFD	Computing Fluid Dynamics
SOD	Standoff Distance
KW	Kerf width
KT	Kerf-Taper
KTA	Kerf-Taper Angle
MTH	Material thickness
HV	Vickers Hardness
SEM	Scanning Electron Microscope

---

## ТЕОРИЈСКО И ЕКСПЕРИМЕНТАЛНО ИСТРАЖИВАЊЕ ЗОНЕ РЕЗАЊА НАСТАЛЕ ПРИМЕНОМ АУЈ ПРОЦЕСА

**А. Патирнак, Р.Г. Рипчану, И.Н. Рамадан**

Примењен је АУЈ процес у циљу теоријског и експерименталног истраживања утицаја воденог млаза на метални материјал који се користи за израду опреме за нафтна поља. Истражено је колико расипање млаза има утицаја на ширину реза и суседну регију. Коришћени материјал је метал P275NL2, квалитетна легура челика ниске температуре, који се користи у петрохемијској индустрији. Експеримент са воденим млазом је изведен на машини за резање YCWJ-380-1520 у претходно дефинисаним радним условима. У теоријском истраживању је на геометријском моделу коришћена CFD симулација са планарним 2D протоком флуида. Испитивана је графичка корелација између исхода симулације и експерименталних резултата, преклапање теоријског истраживања брзине резања и граница брзине отврдњавања непосредно уз рез.